Journal of Electrical and Electronic Engineering
2022; 10(1): 31-38
http://www.sciencepublishinggroup.com/j/jeee
doi: 10.11648/j.jeee.20221001.14
ISSN: 2329-1613 (Print); ISSN: 2329-1605 (Online)

Fiber Fuse Simulation in Double-Clad Fibers for High-Power Fiber Lasers

Yoshito Shuto

Ofra Project, Iruma City, Japan

Email address:
ofra@tuba.ocn.ne.jp

To cite this article:
Yoshito Shuto. Fiber Fuse Simulation in Double-Clad Fibers for High-Power Fiber Lasers. *Journal of Electrical and Electronic Engineering*. Vol. 10, No. 1, 2022, pp. 31-38. doi: 10.11648/j.jeee.20221001.14

Received: January 25, 2022; **Accepted**: February 9, 2022; **Published**: February 16, 2022

Abstract: Rare-earth-doped optical fibers are one of the most promising solid-state lasers. In these fiber lasers, a cladding-pumping scheme using double-clad fibers is utilized to increase the overall conversion efficiency of pumping light. To maintain acceptable beam quality, the low-numerical aperture large-mode-area fibers is effective for the double-clad fibers because the effects of stimulated Raman scattering can be reduced via the corresponding reduction in the power density in the large fiber core. For the large-mode-area double-clad fibers, fiber fuse propagation was investigated theoretically by the explicit finite-difference method using the thermochemical SiO_x production model. In the calculation, we assumed the fiber to be in an atmosphere and that part (40 μm in length) of the core was heated to a temperature of 2,923 K. The threshold power for the double-clad fiber with the core radius of 10 μm was 1.6 W at 1.080 μm and it was close to the experimental value. The power dependence of the velocity of fiber fuse propagation was calculated for the double-clad fibers with the core radius of 10 and 15 μm. The calculated velocities were in fair agreement with the experimental values observed in the input power range from 1 kW to 3.5 kW at 1.080 μm.

Keywords: Fiber Laser, Fiber Fuse Phenomenon, Double-Clad Fiber, Finite-Difference Technique

1. Introduction

Rare-earth-doped optical fibers are one of the most promising solid-state lasers for efficient diode-pumped high power continuous-wave (CW) and fiber chirped-pulse amplification (CPA) laser systems. The output power from the ytterbium (Yb)-doped fiber lasers has abruptly increased over the past decade [1-6]. CW laser oscillation in a Yb-doped single-mode optical fiber was first observed by Hanna *et al.* in 1988 [7]. Extensive work on laser operation of Yb^{3+} ion in silica fibers was reported by several research institutes [8-14]. An attractive feature of Yb^{3+}-doped silica fiber is that it provides a very broad fluorescence in the 1 μm region without excited-state absorption thus offering the potential of broadly tunable laser operation. Hanna *et al.* reported smooth continuous tuning from 1.010 μm to 1.162 μm, but only with low output powers of < 20 mW [9].

The simplicity of the energy level structure of Yb^{3+} gives freedom from excited-state absorption, concentration quenching, and multiphoton nonradiative decay [13, 14]. These features combined with small energy defect between pumping and emission photons allow highly efficient conversion from the absorbed photons.

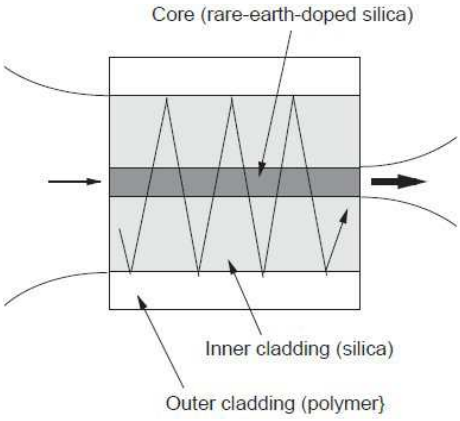

Figure 1. *Schematic of cladding pumping in the DCF.*

The overall conversion efficiencies are limited by the launch efficiency of the pump beam into the single-mode fiber core, and high conversion efficiencies (about 70% [13])

from 0.975 μm pump light are obtained in Yb^{3+}-doped silica fiber by using a cladding-pumping scheme [15] to ensure that virtually all of the incident pump power is absorbed in the doped fiber core.

The cladding-pumping scheme can be realized using double-clad fibers (DCFs), as shown in Figure 1. In a double-clad configuration, light focused into the inner cladding is absorbed by the Yb^{3+}-doped fiber core as the pump light proceeds down the fiber. This allows the use of multimode pump sources and relatively simple focusing systems for efficient coupling. High output power of 500 mW for 0.975 μm pump light was obtained by Pask *et al*. in 1994 using a cladding-pumped Yb^{3+}-doped DCF [13]. Higher power DCFs have also been reported by several research institutes [16-20].

Diffraction-limited beam quality from Yb-doped fiber laser with 135 W output power was demonstrated by Platonov *et al*. who used DCFs with relatively small core diameter of 9 μm [20]. They found that the output power was limited by the onset of stimulated Raman scattering. To overcome this restriction, the concept of low-numerical aperture large-mode-area (LMA) fibers [21, 22] is effective because the effects of Raman scattering can be reduced via the corresponding reduction in the power density in the large fiber core. With regard to optical damage to the end faces, a large-core design is preferred while maintaining acceptable beam quality. The core diameter needed to maintain single-mode transmission depends on a numerical aperture (NA); the smaller the NA, the larger the diameter of a core that could support single-mode transmission. Typical LMA fibers used in the CW laser operation have core diameters of 20-40 μm and an NA of < 0.09 [23-27]. High output power of > 200 W in the CW laser operation has been reported using cladding-pumped Yb-doped and/or Nd+Yb-doped LMA fibers [23-40].

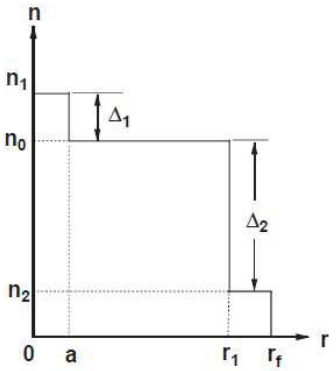

Figure 2. *Refractive-index profile of a DCF.*

On the other hand, it is extremely challenging to increase the fiber core size while retaining the excellent beam quality because fibers with large core size allow propagation of several transversal modes, except for the fundamental mode (FM). As a result, the beam quality of these fibers is influenced by the existence of a higher-order mode (HOM). Wirth *et al.* reported the generation of 1,250 W of narrow linewidth (80 pm) nearly diffraction-limited radiation by a Yb-doped photonic crystal fiber amplifier [41]. They found that the beam quality factor M^2 was about 1.3 and below for output power level up to approximately 1,250 W, and then it increased rapidly to large values of 1.85-1.95 at power level above 1,250 W. It was found that a degradation of beam quality above threshold power (1,250 W) was responsible to superposition of the HOM (LP_{11} mode) on the FM (LP_{01} mode) [41].

This phenomenon of transverse mode instability (TMI) was observed in many fiber lasers and amplifiers under CW and pulsed-pump mode of operation [33, 34, 42-61]. It causes the output beam profile fluctuations in a seemingly chaotic way between the FM and one (or more) HOM.

Although the exact mechanism ultimately causing the energy transfer between the FM and HOM and dynamic behavior of the beam fluctuations is still under discussion, a (quasi-static) thermally-induced index grating [62-64] is the most plausible explanation for the TMI. Recently, Jauregui *et al*. have proposed a novel technique for stabilizing the output beam of a fiber laser system operating above the mode instability threshold [58]. This technique, which relies on a modulation of the pump power, can wash out the thermally-induced refractive index gratings and improve power and beam stability at powers up to twice the normal threshold for onset of the instability [58].

One of the problems other than the TMI arising from high power injection in Yb-doped DCFs is the probability of detonating the fiber fuse effect. In this article, we describe the results of some numerical calculations related to the fiber fuse effects in the DCFs for high-power fiber lasers.

2. Fiber Fuse Effect in DCFs

The first fiber fuse ignition was observed in an Yb-doped DCF with a core radius *a*~5.25 μm by Wang *et al.* in 2008 [65] and then the fiber fuse effect was observed in a Er-doped fiber [66] and Yb-doped bismuthate glass waveguide laser [67].

Recently, several fiber fuse experiments have been conducted on the Yb-doped DCFs for high-power fiber lasers by Zhang *et al.* (*a* = 15 μm) at 1.064 μm [68], Sun *et al.* (*a* = 10 and 15 μm) and Xiao *et al.* (*a* = 10 μm) at 1.080 μm [69, 70], respectively.

2.1. Parameters of DCFs

The refractive-index profile of the DCFs used by Zhang *et al.*, Sun *et al.*, and Xiao *et al.* is shown in Figure 2. In this figure, n_0, n_1 and n_2 are the refractive indices in the core, inner cladding, and outer cladding, respectively. The relative refractive-index differences Δ_1 and Δ_2 are defined as

$$\Delta_1 = \frac{(n_1^2 - n_0^2)}{2n_1^2} \sim \frac{(n_1 - n_0)}{n_1} \quad (1)$$

$$\Delta_2 = \frac{(n_0^2 - n_2^2)}{2n_0^2} \sim \frac{(n_0 - n_2)}{n_0} \quad (2)$$

The DCFs have a 20-30-μm-diameter Yb-doped silica glass core, a 400-μm-diameter inner cladding, and a 500-μm-

diameter outer cladding consisting of a low- refractive-index polymer [68, 70]. Furthermore, Jeong *et al.* reported that the NA (= $n_1\sqrt{2\Delta_1}$) of the core is very small (< 0.05) and the NA (= $n_0\sqrt{2\Delta_2}$) of the inner cladding is 0.48 [27]. From these NA values, we estimated Δ_1 to be smaller than 0.05% and Δ_2 ~5.5%.

The parameters of the DCFs used in the fiber fuse calculation are shown in Table 1.

Table 1. *Parameters of the DCFs.*

Parameters	Unit	DCF10	DCF15
Δ_1	%	0.030	0.013
Δ_2	%	5.50	5.50
a	μm	10	15
r_1	μm	200	200
r_f	μm	250	250
A_{eff}	μm^2	477	1,097

In the following, the DCFs with a = 10 and 15 μm are referred to as DCF10 and DCF15, respectively.

In this table, A_{eff} is the effective cross-sectional area at the wavelength λ_0 = 1.080 μm defined as

$$A_{eff} = \pi\omega^2 \tag{3}$$

where ω is the mode field radius at λ_0. This ω is defined as [71]

$$\frac{\omega}{a} = 0.65 + \frac{1.619}{V^{3/2}} + \frac{2.879}{V^6} \tag{4}$$

where V is the normalized frequency of the optical fiber. V is given by

$$V = 2\pi a\, n_1\sqrt{2\Delta_1}\ /\ \lambda_0 \tag{5}$$

2.2. Fiber Fuse Initiation in DCFs

Fiber fuse was observed in Yb-doped DCFs operated in a master oscillator power amplifier (MOPA) configuration [65, 68-70]. Wang *et al.* reported that the fiber fuse was initiated at the fiber end surface through physically adhered wet-alumina particles and/or the clusters of them interacting with high-power laser light in the core region [65]. Xiao *et al.* prepared an initiation point on a section of DCF near the output end where the polymer coating (outer cladding) was removed, and a piece of metal as absorptive material was manually put on the exposed inner cladding. The fiber fuse was initiated at this point when the maximum power of 3 kW passed through the point [70]. In these cases, it was considered that fiber fuse was generated in the Yb-doped core layer owing to thermally decomposition of SiO_2 (accordingly thermochemical SiO_x production) [65, 70].

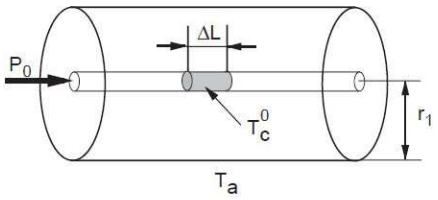

Figure 3. *Schematic view of the hot zone in the core layer.*

In the following subsection, we describe the unsteady-state thermal conduction process in the DCFs theoretically by the explicit finite-difference method on the basis of the thermochemical SiO_x production model [72].

2.3. Fiber Fuse Calculation of DCFs

We assume that the DCF is in an atmosphere of $T = T_a$ and r_1 of the DCF is 200 μm (see Table 1). We also assume that part of the core layer is heated and has a length of ΔL (= 40 μm) and a temperature of T^0_c (> T_a), as shown in Figure 3.

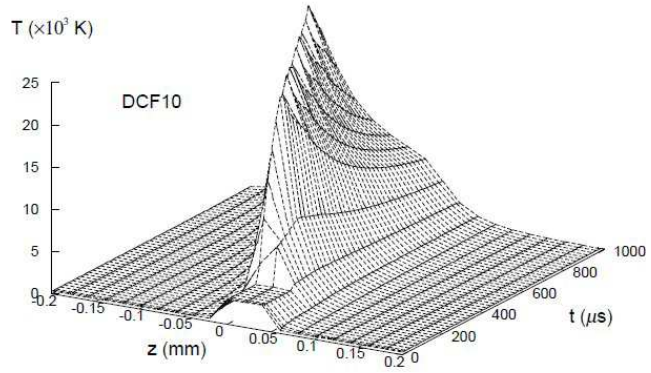

Figure 4. *Core center temperature distribution in the longitudinal direction of DCF10 up to 1,000 μs after the incidence of laser light with P_0 = 2 W and λ_0 = 1.080 μm.*

In the calculation, we set the time interval δt to 10 ns, the step size along the r axis δr to $r_1/20$, and the step size along the z axis δz to 20 μm and assumed that T^0_c = 2,923 K and T_a = 298 K.

To investigate the formation process of the fiber fuse in the DCF10, we calculated the change in the temperature at the core center position with time after the incidence of laser power of 2 W at λ_0 = 1.080 μm. The calculated results are shown in Figure 4.

As shown in this figure, the core center temperature at the end of the hot zone (z = 0 mm) increases to a large value of > 1×10^4 K in the 180 μs after the 2 W laser light incidence. Although a thermal wave with a peak temperature of higher than 2×10^4 K is generated at the end of the hot zone, it was found that this thermal wave does not propagate in the negative z direction with the passage of time until t = 360 μs, and thereafter propagation behavior was observed (see Figure 4). Such a stationary thermal wave was reported by Kashyap [73].

We estimated the changes in the temperature T (0, z) at the core center (r = 0 μm) in the DCF10 and DCF15 at t = 1 ms after the incidence of laser light with λ_0 = 1.080 μm and initial power P_0 = 0-3 W and 0-6 W.

The calculated changes in the temperature at the core center position are shown in Figures 5 and 6. When the power of the light entering the DCF10 increases from 1.5 W to 1.6 W, the peak temperature rises from 2,923 to 21,000 K, and thereafter, propagation behavior was observed in the negative z direction with increasing P_0, as shown in Figure 5.

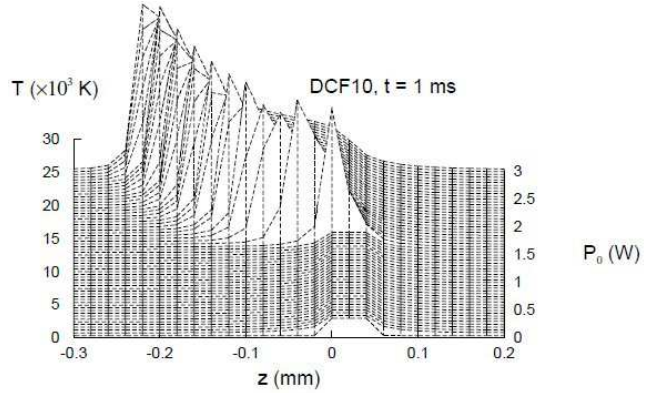

Figure 5. *Core center temperature distribution in the longitudinal direction of the DCF10 after 1 ms with P_0 = 0-3 W and λ_0 = 1.080 μm.*

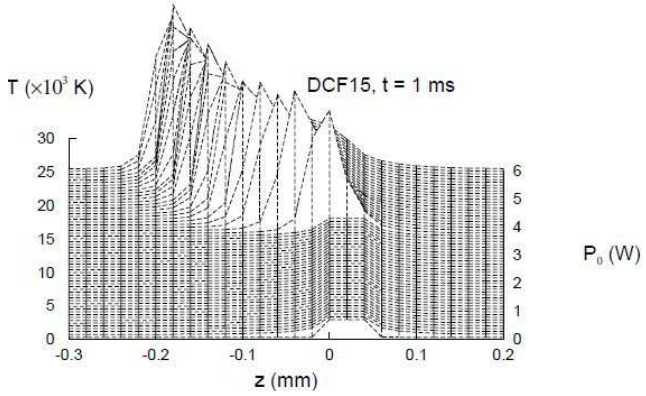

Figure 6. *Core center temperature distribution in the longitudinal direction of the DCF15 after 1 ms with P_0 = 0-6 W and λ_0 = 1.080 μm.*

The characteristic P_0 value of 1.6 W is the threshold power P_{th} of the DCF10. This value is close to the experimental P_{th} value (about 2 W [68]) for the DCF with a~5.25 μm. The P_{th} of the DCF15 is determined as 3.7 W in the same manner as the DCF10, as shown in Figure 6. This value is two times larger than that of the DCF10 because the A_{eff} value (1,097 μm^2) of the DCF15 is larger than that (477 μm^2) of the DCF10 (see Table 1).

Next, we estimated the temperature field of the core center of the DCF10 along the z direction at t = 0.2 ms and 0.5 ms after the incidence of laser light with P_0 = 1.3 kW and λ_0 = 1.080 μm. The calculated results are shown in Figures 7 and 8. As shown in Figure 7, the core center temperature near the end of the hot zone (z = -1.80 mm) changes abruptly to a high value of about 2.8×10^5 K after 0.2 ms. This rapid rise in the temperature initiates the fiber fuse propagation, as shown in 8. After 0.5 ms, the high-temperature front in the core layer reaches a z value of -4.52 mm. The average propagation velocity V_f is estimated to be 9.07 m/s using these data. This V_f of the DCF10 is close to the value of 8.75 m/s measured by Sun *et al.* [69].

As shown in Figures 7 and 8, a sharp temperature peak located near the light source and a relatively high temperature plateau of about 2×10^4 K extending over 2-4 mm behind the sharp peak can be clearly seen. These regions located in the core are hotter than the surrounding cladding regions.

We examined the P_0 dependence of the V_f values for the DCF10 and DCF15 at λ_0 = 1.080 μm. The results are shown in Figure 9. In this figure, the open circles and open triangle are the data reported by Sun *et al.* [69] and the closed circle is the datum reported by Xiao *et al.* [70]. As shown in Figure 9, the calculated V_f values are close to the experimental values.

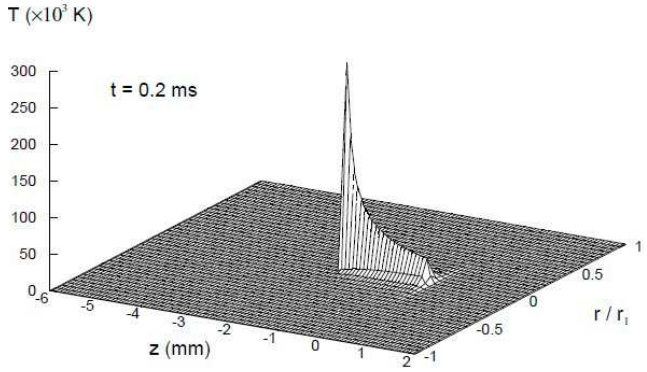

Figure 7. *Temperature field in DCF10 after 0.2 ms when P_0 = 1.3 kW at λ_0 = 1.080 μm.*

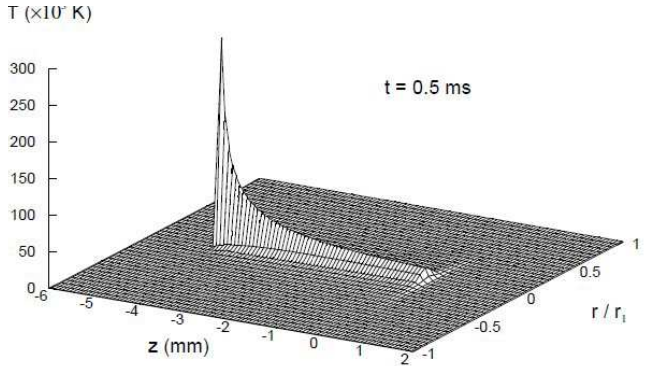

Figure 8. *Temperature field in DCF10 after 0.5 ms when P_0 = 1.3 kW at λ_0 = 1.080 μm.*

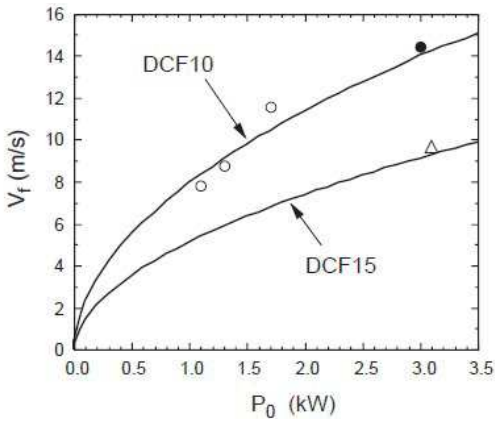

Figure 9. *Power dependence of the fiber fuse propagation velocities of the DCF10 and DCF15 at λ_0 = 1.080 μm. The open circles and open triangle indicate the data reported by Sun et al. [69] and the closed circle indicates the datum reported by Xiao et al. [70].*

2.4. Power Dependence of Cavity Interval

Sun *et al.* reported the interval Λ and length l values of the cavities at P_0 = 1.1, 1.3, 1.7 and 3.1 kW [69]. The

experimental Λ and l values are listed in Table 2 together with the reported V_f values.

The relationship between the propagation velocity V_f and the interval Λ is given by

$$\Lambda = \emptyset V_f \quad (6)$$

where ϕ is the period of the fiber fuse.

We estimated the ϕ values using Eq. (6) and the data listed in Table 2 at P_0 = 1.1, 1.3, 1.7 and 3.1 kW. The calculated results are shown in Figure 10.

Table 2. *Cavity intervals and propagation velocities of fiber fuse [69].*

P_0 (kW)	V_f (m/s)	Λ (μm)	l (μm)
1.1	7.82	64.4	26.1
1.3	8.75	167.4	57.6
1.7	11.58	233.1	73.8
3.1	9.68	188.1	96.2

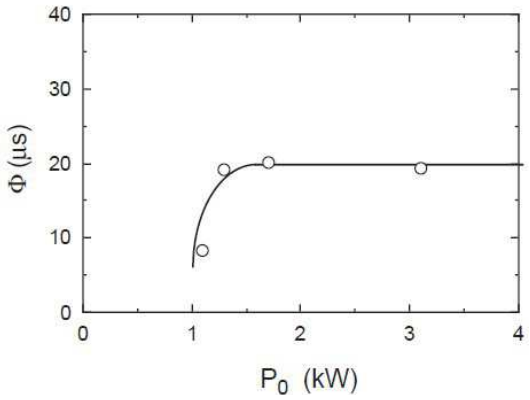

Figure 10. *Relationship between the period ϕ and the input power P_0. The open circles are the values calculated using the data reported by Sun et al. [71].*

As shown in Figure 10, ϕ increases with increasing P_0 and gradually approaches to a constant value of about 20 μs at P_0 > 1.3 kW. This value (20 μs) is close to the ϕ (19 μs) observed at P_0 > 6 W in the conventional SMFs (see Figure on page 283 in [74]).

The period ϕ corresponds to the time required for the formation of one cavity during fiber fuse propagation [75] and ϕ~20 μs is the one under the thermodynamically stable condition of fiber fuse propagation.

Therefore, it can be seen from Figure 10 that fiber fuse propagation in the DCF10 and DCF15 is stabilized at P_0 > 1.3 kW.

It is well known that the fiber fuse phenomenon occurs when a light-absorbing substance (such as dust) is applied to the end face of a fiber and/or when a small region of a fiber core is melted by a fusion splicer using arc discharge [72].

Furthermore, failures at bends are caused by the light that leaks from the core when the fiber is accidentally tightly bent under high power [76]. In order to suppress HOMs, a bend radius of the DCF is controlled to increase the bend loss of LP_{11} mode while keeping a low bend loss of LP_{00} mode [27]. Further investigation focused on the relationship between the fiber fuse effect and the bending loss in DCFs is needed to improve the reliability of DCFs for high-power fiber lasers.

3. Conclusion

For the large-mode-area double-clad fibers (DCFs), fiber fuse propagation was investigated theoretically by the explicit finite-difference method using the thermochemical SiO_x production model. The threshold power for the DCF with the core radius of 10 μm was 1.6 W at 1.080 μm and it was close to the experimental value. The power dependence of the velocity of fiber fuse propagation was calculated for the DCFs with the core radius of 10 and 15 μm. The calculated velocities were in fair agreement with the experimental values observed at 1.080 μm.

References

[1] Richardson D. J., Nilsson J., and Clarkson W. A. (2010). High power fiber lasers: current status and future perspectives. J. Opt. Soc. Am. B, 27 (11), B63-B92.

[2] Tünnermann A., Schreiber T., and Limpert J. (2010). Fiber lasers and amplifiers: an ultrafast performance evolution. Appl. Opt., 49 (25), F71-F78.

[3] Jauregui C., Limpert J., and Tünnermann A. (2013). High-power fibre lasers. Nat. Photonics, 7, 861-867.

[4] Fermann M. E. and Hartl I. (2013). Ultrafast fibre lasers. Nat. Photonics, 7, 868-874.

[5] Zervas M. N. and Codemand C. A. (2014). High power fiber lasers: a review. IEEE J. Selected Topics Quantum Electron., 20 (5), 0904123.

[6] Shi W., Fang Q., Zhu X., Norwood R. A., and Peyghambarian N. (2014). Fiber lasers and their applications. Appl. Opt., 53 (28), 6554-6568.

[7] Hanna D. C., Percival P. M., Perry I. R., Smart R. G., Suni P. J., Townsend J. E., and Tropper A. C. (1988). Continuous-wave oscillation of a monomode ytterbium-doped fibre laser. Electron. Lett., 24 (17), 1111-1113.

[8] Armitage J. R., Wyatt R., Ainslie B. J., and Craig-Ryan S. P. (1989). Highly efficient 980 nm operation of an Yb^{3+}-doped silica fibre laser. Electron. Lett., 25 (5), 298-299.

[9] Hanna D. C., Percival P. M., Perry I. R., Smart R. G., Suni P. J., and Tropper A. C. (1990). An ytterbium-doped monomode fibre laser: broadly tunable operation from 1.010 μm to 1.162 μm and three-level operation at 974 nm. J. Mod. Opt., 37 (4), 1111-1113.

[10] Allain J. Y., Monerie M., and Poignant H. (1992). Ytterbium-doped fluoride fibre laser operating at 1.02 μm. Electron. Lett., 28 (11), 988-989.

[11] Machechnie C. J., Barnes W. L., Hanna D. C., and Townsend J. E. (1993). High power ytterbium (Yb^{3+})-doped fibre laser operating in the 1.12 μm region. Electron. Lett., 29 (1), 52-53.

[12] Allain J. Y., Bayon J. F., Monerie M., Bernage P., and Niay P. (1993). Ytterbium-doped silica fibre laser with intracore Bragg gratings operating at 1.02 μm. Electron. Lett., 29 (3), 988-989.

[13] Pask H. M., Archambault J. L., Hanna D. C., Reekie L., Russell P. St. J., Townsend J. E., and Tropper A. C. (1994). Operation of cladding-pumped Yb^{3+}-doped silica fibre lasers in 1 μm region. Electron. Lett., 30 (11), 863-865.

[14] Pask H. M., Carman R. J., Hanna D. C., Tropper A. C., Mackechnie C. J., Barber P. R., and Dawes J. M. (1995). Ytterbium-doped silica fiber lasers: versatile sources for the 1-1.2 μm region. IEEE J. Selected Topics Quantum Electron., 1 (1), 2-13.

[15] Snitzer E., Po H., Hakimi F., Tumminelli R., and McCollum B. C. (1988). Double clad, offset core Nd fiber laser. Conf. on Optical Fiber Sensors, PD5-1.

[16] Inniss D., DiGiovanni D. J., Strasser T. A., Hale A., Headley C., Stentz A. J., Pedrazzani R., Tipton D., Kosinski S. G., Brownlow D. L., Quoi K. W., Kranz K. S., Huff R. G., Espindola R., LeGrange J. D., and Jacobovitz-Veselka G. (1997). Ultrahigh-power single-mode fiber lasers from 1.065 to 1.472 μm using Yb-doped cladding-pumped and cascaded Raman lasers. Proc. Conf. on Lasers and Electro-Optics (CLEO), CPD31.

[17] Muendel M., Engstrom B., Kea D., Laliberte B., Minns R., Robinson R., Rockney B., Zhang Y., Colins R., Gavrilovic P., and Rowley A. (1997). 35-Watt CW singlemode ytterbium fiber laser at 1.1 μm. Proc. Conf. on Lasers and Electro-Optics (CLEO), CPD30.

[18] Boggavarapu D., Caffey D., He X., Gupta S., Srinivasan S., Pleak R., and Patel R. (1998). Ultrahigh-power laser diode array pump source for fiber lasers. Optical Fiber Commun. Conf. (OFC'98), TuH7.

[19] Dominic V., MacCormack S., Waarts R., Sanders S., Bicknese S., Dohle R., Wolak E., Yeh P. S., and Zucker E. (1999). 110 W fibre laser. Electron. Lett., 35 (14), 1158-1160.

[20] Platonov N. S., Gapontsev D. V., Gapontsev V. P., and Shumilin V. (2002). 135 W CW fiber laser with perfect single mode output. Proc. Conf. on Lasers and Electro-Optics (CLEO), CPDC3.

[21] Broderick N. G. R., Offerhaus H. L., Richardson D. J., Sammut R. A., Caplen J., and Dong L. (1999). Large mode area fibers for high power applications. Opt. Fiber Technol., 5, 185-196.

[22] Alvarez-Chavez J. A., Offerhaus H. L., Nilsson J., Turner P. W., Clarkson W. A., and Richardson D. J. (2000). High-energy, high-power ytterbium-doped Q-switched fiber laser. Opt. Lett., 25 (1), 37-39.

[23] Jeong Y., Sahu J. K., Williams R. B., Richardson D. J., Furusawa K., and Nilsson J. (2003). Ytterbium-doped large-core fibre laser with 272 W output power. Electron. Lett., 39 (13), 977-978.

[24] Limpert J., Liem A., Zellmer H., and Tünnerman A. (2003). 500 W continuous-wave fibre laser with excellent beam quality. Electron. Lett., 39 (8), 645-647.

[25] Liu C. -H., Ehlers B., Doerfel F., Heinemann S., Carter A., Tankala K., Farroni J., and Galvanauskas A. (2004). 810 W continuous-wave and single-transverse-mode fibre laser using 20 μm core Yb-doped double-clad fibre. Electron. Lett., 40 (23), 1471-1472.

[26] Jeong Y., Sahu J. K., Payne D. N., and Nilsson J. (2004). Ytterbium-doped large-core fibre laser with 1 kW of continuous-wave output power. Electron. Lett., 40 (8), 470-471.

[27] Jeong Y., Sahu J. K., Payne D. N., and Nilsson J. (2004). Ytterbium-doped large-core fiber laser with 1. 36 kW continuous-wave output power. Opt. Express, 12 (25), 6088-6092.

[28] He B., Zhou J., Lou Q., Xue Y., Li Z., Wang W., Dong J., Wei Y., and Chen W. (2010). 1. 75-kilowatt continuous-wave output fiber laser using homemade ytterbium-doped large-core fiber. Microwave Opt. Technol. Lett., 52 (7), 1668-1671.

[29] Jeong Y., Boyland A. J., Sahu J. K., Chung S., Nilsson J., and Payne D. N. (2009). Multi-kilowatt single-mode ytterbium-doped large-core fiber laser. J. Opt. Soc. Korea, 13 (4), 416-422.

[30] Huang L., Wang W., Leng J., Guo S., Xu X., and Cheng X. (2014). Experimental investigation on evolution of the beam quality in a 2-kW high power fiber amplifier. IEEE Photon. Technol. Lett., 26 (1), 33-36.

[31] Khitrov V., Minelly J. D., Tumminelli R., Petit V., and Pooler E. S. (2014). 3 kW single-mode direct diode-pumped fiber laser. Proc. Soc. Photo-Opt. Instrum. Eng., 8961, 89610V-1-89610V-6.

[32] Yu H., Zhang H., Lv H., Wang X., Leng J., Xiao H., Guo S., Zhou P., Xu X., and Chen J. (2015). 3. 15 kW direct diode-pumped near diffraction-limited all-fiber-integrated fiber laser. Appl. Opt., 54 (14), 4556-4560.

[33] Beier F., Hupel C., Nold J., Kuhn S., Hein S., Ihring J., Sattler B., Haarlammert N., Schreiber T., Eberhardt R., and Tünnermann A. (2016). Narrow linewidth, single mode 3 kW average power from a directly diode pumped ytterbium-doped low NA fiber amplifier. Opt. Express, 24 (6), 6011-6020.

[34] Beier F., Hupel C., Kuhn S., Hein S., Nold J., Proske F., Sattler B., Liem A., Jauregui C., Limpert J., Haarlammert N., Schreiber T., Eberhardt R., and Tünnermann A. (2017). Single mode 4. 3 kW output power from a diode-pumped Yb-doped fiber amplifier. Opt. Express, 25 (13), 14892-14899.

[35] Su R., Tao R., Wang X., Zhang H., Ma P., Zhao P., and Xu X. (2017). 3. 7 kW monolithic narrow linewidth single mode fiber laser through simultaneously suppressing nonlinear effects and mode instability. Laser Phys. Lett., 14, 085102.

[36] Wang Y., Gao C., Tang X., Zhan H., Peng K., Ni L., Liu S., Li Y., Guo C., Wang X., Zhang L., Yu J., Jiang L., Lin H., Wang J., Jing F., and Lin A. (2018). 30/900 Yb-doped aluminophosphosilicate fiber presenting 6. 85-kW laser output pumped with commercial 976-nm laser diodes. IEEE J. Lightwave Technol., 36 (16), 3396-3402.

[37] Xiao Q., Li D., Huang Y., Wang X., Wang Z., Tian J., Yan P., and Gong M. (2018). Directly diode and bi-directional pumping 6 kW continuous-wave all-fibre laser. Laser Phys., 28, 125107.

[38] Shima K., Ikoma S., Uchiyama K., Takubo Y., Kashiwagi M., and Tanaka D. (2018). 5-kW single stage all-fiber Yb-doped single-mode fiber laser for material processing. Proc. Soc. Photo-Opt. Instrum. Eng., 10512, 105120C-1-105120C-6.

[39] Lin H., Xu L., Li C., Shu Q., Chu Q., Xie L., Guo C., Zhao P., Li Z., Wang J., Jing F., and Tang X. (2019). 10. 6 kW high-brightness cascade-end-pumped monolithic fiber lasers directly pumped by laser diodes in step-index large mode area double cladding fiber. Results in Phys., 14, 102479.

[40] Ye Y., Yang B., Wang P., Zeng L., Xi X., Shi C., Zhang H., Wang X., Zhou P., and Xu X. (2021). Industrial 6 kW high-stability single-stage all-fiber laser oscillator based on conventional large mode area ytterbium-doped fiber. Laser Phys., 31, 035104.

[41] Wirth C., Schreiber T., Rekas M., Tsybin I., Peschel T., Eberhardt R., and Tünnermann A. (2010). High-power linear-polarized narrow linewidth photonic crystal fiber amplifier. Proc. Soc. Photo-Opt. Instrum. Eng., 7580, 75801H-1-75801H-6.

[42] Eidam T., Hanf S., Seise E., Andersen T. V., Gabler T., Wirth C., Schreiber T., Limpert J., and Tünnermann A. (2010). Femtosecond fiber CPA system emitting 830 W average output power. Opt. Lett., 35 (2), 94-96.

[43] Eidam T., Wirth C., Jauregui C., Stutzki F., Jansen F., Otto H. -J., Schmidt O., Schreiber T., Limpert J., and Tünnermann A. (2011). Experimental observations of the threshold-like onset of mode instabilities in high power fiber amplifiers. Opt. Express, 19 (14), 13218-13224.

[44] Stutzki F., Otto H. -J., Jansen F., Gaida C., Jauregui C., Limpert J., and Tünnermann A. (2011). High-speed modal decomposition of mode instabilities in high-power fiber lasers. Opt. Lett., 36 (23), 4572-4574.

[45] Karow M., Tünnermann H., Neumann J., Kracht D., and Weβels P. (2012). Beam quality degradation of a single-frequency Yb-doped photonic crystal fiber amplifier with low mode instability threshold power. Opt. Lett., 37 (20), 4242-4244.

[46] Laurila M., Johansen M. M., Hansen K. R., Alkeskjold T. T., Broeng J., and Lægsgaard J. (2012). Distributed mode filtering rod fiber amplifier delivering 292 W with improved mode stability. Opt. Express, 20 (5), 5742-5753.

[47] Haarlammert N., de Vries O., Liem A., Kliner A., Peschel T., Schreiber T., Eberhardt R., and Tünnermann A. (2012). Build up and decay of mode instability in a high power fiber amplifier. Opt. Express, 20 (12), 13274-13283.

[48] Otto H. -J., Stutzki F., Jansen F., Eidam T., Jauregui C., Limpert J., and Tünnermann A. (2012). Temporary dynamics of mode instabilities in high-power fiber lasers and amplifiers. Opt. Express, 20 (14), 15710-15722.

[49] Otto H. -J., Jauregui C., Stutzki F., Jansen F., Limpert J., and Tünnermann A. (2013). Controlling mode instabilities by dynamic mode excitation with an acousto-optic deflector. Opt. Express, 21 (14), 17285-17298.

[50] Johansen M. M., Laurila M., Maack M. D., Noordegraaf D., Jakobsen C., Alkeskjold T. T., and Lægsgaard J. (2013). Frequency resolved transverse mode instability in rod fiber amplifiers. Opt. Express, 21 (19), 21847-21856.

[51] Brar K., Savage-Leuchs M., Henrie J., Courtney S., Dilley C., Afzail R., and Honea E. (2014). Threshold power and fiber degradation induced modal instabilities in high power fiber amplifiers based on large mode area fibers. Proc. Soc. Photo-Opt. Instrum. Eng., 8961, 89611R-1-89611R-9.

[52] Robin C., Dajani I., and Pulford B. (2014). Modal instability-suppressing, single-frequency photonic crystal fiber amplifier with 811 W output power. Opt. Lett., 39 (3), 666-669.

[53] Otto H. -J., Klenke A., Jauregui C., Stutzki F., Limpert J., and Tünnermann A. (2014). Scaling the mode instability threshold with multicore fibers. Opt. Lett., 39 (9), 2680-2683.

[54] Kuznetsov M., Vershinin O., Tyrtyshnyy V., and Antipov O. (2014). Low-threshold mode instability in Yb^{3+}-doped few-mode fiber amplifiers. Opt. Express, 22 (24), 29714-29725.

[55] Yang B., Zhang H., Shi C., Wang X., Zhou P., Xu X., Chen J., Liu Z., and Lu Q. (2016). Mitigating transverse mode instability in all-fiber laser oscillator and scaling power up to 2. 5 kW employing bidirectional-pump scheme. Opt. Express, 24 (24), 27828-27835.

[56] Malleville M. -A., Dauliat R., Benoit A., Leconte B., Darwich D., du Jeu R., Jamier R., Schuster K., and Roy P. (2017). Experimental study of the mode instability onset threshold in high-power FA-LPF lasers. Opt. Lett., 42 (24), 5230-5233.

[57] Alekseev D., Tyrtyshnyy V., Kuznetsov M., and Antipov O. (2018). Transverse-mode instability in high-gain few-mode Yb^{3+}-doped fiber amplifiers with a 10 μm core diameter with or without backward reflection. IEEE J. Selected Topics Quantum Electron., 24 (3), 5100608.

[58] Jauregui C., Stihler C., Tünnermann A., and Limpert J. (2018). Pump-modulation-induced beam stabilization in high-power fiber laser systems above the mode instability threshold. Opt. Express, 26 (8), 10691-10704.

[59] Stihler C., Jauregui C., Tünnermann A., and Limpert J. (2018). Phase-shift evolution of the thermally-induced refractive index grating in high-power fiber laser systems induced by pump-power variations. Opt. Express, 26 (15), 19489-19497.

[60] Scarnera V., Ghiringhelli F., Malinowski A., Codemard C. A., Durkin M. K., and Zervas M. N. (2019). Modal instabilities in high power fiber laser oscillators. Opt. Express, 27 (4), 4386-4403.

[61] Jauregui C., Stihler C., and Limpert J. (2020). Transverse mode stability. Ad. Opt. Photon., 12 (2), 420-484.

[62] Jauregui C., Eidam T., Otto H. -J., Stutzki F., Jansen F., Limpert J., and Tünnermann A. (2012). Temperature-induced index gratings and their impact on mode instabilities in high-power fiber laser systems. Opt. Express, 20 (1), 440-451.

[63] Jauregui C., Eidam T., Otto H. -J., Stutzki F., Jansen F., Limpert J., and Tünnermann A. (2012). Physical origin of mode instabilities in high-power fiber laser systems. Opt. Express, 20 (12), 12912-12925.

[64] Jauregui C., Otto H. -J., Stutzki F., Jansen F., Limpert J., and Tünnermann A. (2013). Passive mitigation strategies for mode instabilities in high-power fiber laser systems. Opt. Express, 21 (16), 19375-19386.

[65] Wang J., Gray S., Walton D., and Zentero L. (2008). Fiber fuse in high power optical fiber. Proc. Soc. Photo-Opt. Instrum. Eng., 7134, 71342E-1-71342E-9.

[66] Domingues F., Frias A. R., Antunes P., Sousa A. O. P., Ferreira R. A. S., and André P. S. (2012). Observation of fuse effect discharge zone nonlinear velocity regime in erbium-doped fibres. Electron. Lett., 48 (20), 1295-1296.

[67] Mary R., Choudhury D., and Kar A. K. (2014). Applications of fiber lasers for the development of compact photonic devices. IEEE J. Selected Topics Quantum Electron., 20 (5), 0902513.

[68] Zhang H., Zhou P., Wang X., Xiao H., and Xu X. (2013). Fiber fuse effect in high-power double-clad fiber laser. Conf. on Lasers and Electro-Optics Pacific Rim (CLEO-PR), WPD-4.

[69] Sun J., Xiao Q., Li D., Wang X., Zhang H., Gong M., and Yan P. (2016). Fiber fuse behavior in kW-level continuous-wave double-clad field laser. Chinese Phys. B, 25 (1), 014204.

[70] Xiao Q., Tian J., Huang Y., Wang X., Wang Z., Li D., Yan P., and Gong M. (2018). Internal features of fiber fuse in a Yb-doped double-clad fiber at 3 kW. Chinese Phys. Lett., 35 (5), 054201.

[71] Marcuse D. (1977). Loss analysis of single-mode fiber splices. Bell Syst. Tech. J., 56 (5), 703-718.

[72] Shuto Y. (2014). Heat conduction modeling of fiber fuse in single-mode optical fibers. J. Photonics, 2014, 645207.

[73] Kashyap R. (2013). The fiber fuse-from a curious effect to a critical issue: a 25th year retrospective. Opt. Express, 21 (5), 6422-6441.

[74] Shuto Y. (2020). Cavity pattern formation and its dynamics of fiber fuse in single-mode optical fibers. J. Informatics Math. Sci., 12 (4), 271-288.

[75] Todoroki S. (2014). Fiber Fuse: Light-Induced Continuous Breakdown of Silica Glass Optical Fiber. NIMS Monographs, Chap. 3, Springer, Tokyo.

[76] Sikora E. S. R., McCartney D. J., Farrow K., and Davey R. (2003). Reduction in fibre reliability due to high optical power. Electron. Lett., 39 (14), 1043-1044.